On the influence of crack shape on effective elasticity of fractured media

Vladimir Grechka*, Ivan Vasconcelos‡, and Mark Kachanov†

* *Shell International Exploration and Production, Inc., 3737 Bellaire Blvd., P. O. Box 481, Houston, TX, 77001-0481, USA*
‡ *Center for Wave Phenomena, Department of Geophysics, Colorado School of Mines, Golden, CO 80401, USA*
† *Department of Mechanical Engineering, Tufts University, Medford, MA 02155, USA*

ABSTRACT

A circle is the basic fracture shape adopted by conventional effective media theories to describe the overall elasticity of cracked solids. As fractures in rocks do not resemble circles, it is important to find out to what extent the available theoretical results are applicable to realistic fracture shapes. To address this issue, we conduct 3D numerical experiments on the so-called digital rocks containing irregular cracks that might be partially closed and might intersect each other. Despite profound deviations of our fracture geometries from circles, we find that basic theoretical results originally developed for penny-shaped cracks remain valid for arbitrary fracture shapes. Based on a series of finite element computations, we show the following:

(1) As far as the effective elasticity is concerned, flat fractures with random in-plane irregularities are accurately represented by circular ones.

(2) Approximate effective elliptical orthotropy established for multiple sets of dry penny-shaped cracks embedded in isotropic host rock holds with the same accuracy for irregular, possibly intersecting fractures.

Key words: irregular cracks, effective media, anisotropy

1 INTRODUCTION

Many years of extensive research and a vast body of literature are devoted to elasticity of solids with penny-shaped cracks (e.g., Bristow, 1960; Walsh 1965a; 1965b; Kachanov, 1980; Hudson, 1980). These efforts have laid the foundation of our current understanding of the effective (or overall) properties of fractured media and identified the quantities that control them. Analyzing many conventional results, however, we might come to a conclusion that they far too often rely on the extremely simple – circular or "penny" – shape of the fractures. Let us take the crack density as an example. This quantity, which is the key for describing the effective elastic behavior of fractured solids, is intimately related to the crack radii and, thus, to circular fractures. On the other hand, all fractures found in natural environments, especially in rocks, have notoriously irregular shapes; these fractures typically intersect each other and might be partially closed. As they do not resemble circles, it remains unclear to what extent the existing theoretical results are applicable to real cracks.

The undeniable presence of irregular fracture geometries obviously challenges the conventional effective media theories and raises a number of questions that do not exist for circular cracks. At least some of them need to be addressed if we want to improve our ability to characterize realistic fractured formations. To illustrate the pertinent issues, consider several sets of planar, irregularly-shaped cracks that have random in-plane orientations and are embedded in an otherwise isotropic background. Then, for example, the following questions might be asked:

Can we replace our irregularly-shaped cracks with the penny-shaped ones that yield approximately the same overall elasticity? If yes, what is the accuracy of such a replacement?

What would be the density of equivalent circular

cracks (defined via their radii) for a given distribution of non-circular fractures?

Multiple sets of dry penny-shaped cracks result in the effective symmetry close to orthorhombic [see Kachanov(1980; 1993) for the theory and Grechka and Kachanov (2006a) for numerical confirmation]. Does the orthotropy[†] hold when the fracture shapes deviate from circles?

Some of these problems were partially addressed by Sevostianov and Kachanov (2002), who studied a number of simple irregular shapes analytically, and by Saenger et al. (2004) and Grechka and Kachanov (2006b), who examined intersecting circular cracks numerically. Here we answer the above questions directly by performing finite element experiments on non-circular fractures. We begin with computing the ratios of normal-to-tangential (averaged in the crack plane) displacement jumps across our irregular fractures. Regardless the fracture shape, we find these ratios to be sufficiently close to that of a penny-shaped crack imbedded in the same background material. An approximate equivalence of the two ratios implies that, on average, flat, irregularly-shaped cracks behave similarly to penny-shaped ones and, therefore, the overall orthotropy can be expected. Next, we numerically calculate the contributions, $\Delta\boldsymbol{c}$, of our irregular, randomly oriented fractures to the effective stiffness and fit these contributions using the analytic solutions, $\Delta\boldsymbol{c}^{\,\mathrm{ps}}(e)$, for penny-shaped cracks (Kachanov et al., 2003) that have unknown crack densities e. We find the values of e that provide an excellent fit of $\Delta\boldsymbol{c}^{\,\mathrm{ps}}(e)$ to $\Delta\boldsymbol{c}$. This indicates that circular cracks can be legitimately used to represent any non-circular ones. Finally, we perform a series of finite element simulations for models with several sets of rectangular fractures to demonstrate that, indeed, their effective anisotropy is orthorhombic despite the deviations of fracture shapes from circles and the presence of multiple crack intersections.

2 EFFECTIVE ELASTICITY OF ROCKS WITH PLANAR FRACTURES

The effective stiffness, $\boldsymbol{c}_e$, and compliance, $\boldsymbol{s}_e$, tensors of a heterogeneous solid (with cracks, in particular) enter Hooke's law that has two equivalent forms,

$$\tau_{ij} = c_{e,\,ijkl}\,\varepsilon_{kl} \quad (i,\,j = 1,\,2,\,3) \tag{1}$$

and

$$\varepsilon_{ij} = s_{e,\,ijkl}\,\tau_{kl} \quad (i,\,j = 1,\,2,\,3)\,, \tag{2}$$

which relate to each other via an obvious equality

$$\boldsymbol{s}_e = \boldsymbol{c}_e^{-1}\,. \tag{3}$$

Here $\boldsymbol{\tau}$ and $\boldsymbol{\varepsilon}$ are the stress and strain tensors, respectively, averaged over the representative volume V, and a summation from 1 to 3 with respect to all repeating subscripts is assumed. Formulation 2 is more appropriate for cracks because they are the sources of extra strains. To emphasize this fact, equation 2 can be rewritten in a more explicit form

$$\begin{aligned}\varepsilon_{ij} &= s_{b,\,ijkl}\,\tau_{kl} + \Delta\varepsilon_{ij}\\ &= (s_{b,\,ijkl} + \Delta s_{ijkl})\,\tau_{kl} \quad (i,\,j = 1,\,2,\,3)\,,\end{aligned} \tag{4}$$

where $\boldsymbol{s}_b$ is the compliance tensor of the host rock,

$$\Delta\varepsilon_{ij} = \Delta s_{ijkl}\,\tau_{kl} \quad (i,\,j = 1,\,2,\,3) \tag{5}$$

is the extra strain due to cracks, and $\Delta\boldsymbol{s}$ is the fracture contribution to the effective compliance.

For a solid containing *flat* fractures, the extra strain $\Delta\boldsymbol{\varepsilon}$ is expressed in terms of the displacement discontinuities $[\boldsymbol{u}] = \boldsymbol{u}^+ - \boldsymbol{u}^-$ across the cracks as (Vavakin and Salganik, 1975; Kachanov, 1980; 1992)

$$\Delta\varepsilon_{ij} = \frac{1}{2\,V}\sum_k \left[\,(n_i\,b_j + b_j\,n_i)\,A\,\right]^{(k)} \quad (i,\,j = 1,\,2,\,3)\,. \tag{6}$$

Here $\boldsymbol{n}$ is the unit crack normal, A is the crack area, $\boldsymbol{b} = \langle[\boldsymbol{u}]\rangle$ is the displacement-discontinuity vector averaged over A, and the sum is taken with respect to all fractures k in volume V. If interactions in the stress fields of different cracks are ignored (the so-called *non-interaction approximation*), $\boldsymbol{b}$ can be expressed through the symmetric, second-rank, excess fracture compliance tensor $\boldsymbol{Z}$ (Schoenberg, 1980; Kachanov, 1992). Tensor $\boldsymbol{Z}$ relates vector $\boldsymbol{b}$ to the uniform traction $\boldsymbol{n}\cdot\boldsymbol{\tau}$ induced at the crack face by the remotely applied stress,

$$b_k = n_i\,\tau_{ij}\,Z_{jk} \quad (k = 1,\,2,\,3)\,. \tag{7}$$

When the host material is isotropic, one of the principal directions of $\boldsymbol{Z}$ always coincides with the crack normal $\boldsymbol{n}$ (Sevostianov and Kachanov, 2002), while the other two, $\boldsymbol{r}$ and $\boldsymbol{t}$, lie in the fracture plane. Consequently, tensor $\boldsymbol{Z}$ becomes diagonal in its natural coordinate frame $[\boldsymbol{n},\,\boldsymbol{r},\,\boldsymbol{t}]$,

$$Z_{ij} = Z_{nn}\,n_i\,n_j + Z_{rr}\,r_i\,r_j + Z_{tt}\,t_i\,t_j \quad (i,\,j = 1,\,2,\,3); \tag{8}$$

no summation with respect to indexes n, r, and t. The eigenvalue $Z_N \equiv Z_{nn}$ is called the *normal* crack compliance, and Z_{rr}, Z_{tt} are the *shear* compliances. They were derived for elliptic cracks by Budiansky and O'Connell (1976).

2.1 Dry circular cracks

Although certain results have been published for ellipsoidal fractures and inclusions (Eshelby, 1957; Budiansky and O'Connell, 1976; Kachanov, 1992; Hudson,

[†] The term "orthotropy," a synonym to "orthorhombic anisotropy," means a medium that possesses orthorhombic symmetry. "Orthotropy" is a noun; the corresponding adjective is "orthotropic."

1994), most progress to date has been made for circular cracks. The rotational symmetry around their normals $\boldsymbol{n}$ leads to independence of the shear compliances on directions within the fracture planes, so two eigenvalues Z_{rr} and Z_{tt} become equal, $Z_{rr} = Z_{tt} \equiv Z_T$. This equivalence, which also holds for *elastically* axisymmetric shapes that include all equilateral polygons, results in the compliance tensor

$$Z_{ij} = Z_N\, n_i\, n_j + Z_T\, (\delta_{ij} - n_i\, n_j)\,, \qquad (i,\, j = 1,\, 2,\, 3)\,, \qquad (9)$$

where δ_{ij} is the Kronecker delta. Substitution of equation 9 into formulae 5–7 yields the non-interaction approximation for the combined contribution $\Delta \boldsymbol{s}$ of multiple cracks to the effective compliance (Kachanov, 1980; 1992; Sayers and Kachanov, 1995; Schoenberg and Sayers, 1995)

$$\Delta s_{ijlm} = \frac{1}{V} \sum_k \Big[\frac{A\, Z_T}{4}\, (n_i\, n_l\, \delta_{jm} + n_i\, n_m\, \delta_{jl} + n_j\, n_l\, \delta_{im} + n_j\, n_m\, \delta_{il}) - A\, (Z_T - Z_N)\, n_i\, n_j\, n_l\, n_m \Big]^{(k)}, \qquad (i,\, j,\, l,\, m = 1,\, 2,\, 3)\,. \qquad (10)$$

Then the fracture contribution, $\Delta \boldsymbol{c}$, to the effective stiffness is

$$\Delta \boldsymbol{c} \equiv \boldsymbol{c}_e - \boldsymbol{c}_b = (\boldsymbol{s}_e)^{-1} - \boldsymbol{c}_b = (\boldsymbol{s}_b + \Delta \boldsymbol{s})^{-1} - \boldsymbol{c}_b\,, \quad (11)$$

where $\boldsymbol{c}_b$ is the stiffness tensor of the isotropic host rock.

The normal and shear compliances for dry circular cracks are (Eshelby, 1957; Budiansky and O'Connell, 1976; Kachanov, 1980)

$$Z_N = \frac{16\, a\, (1 - \nu^2)}{3\, \pi\, E} \qquad (12)$$

and

$$Z_T = \frac{Z_N}{1 - \nu/2}\,, \qquad (13)$$

where a is the fracture radius, and ν and E are the background Poisson's ratio and Young's modulus, respectively. Since $\nu < 1/2$, Z_N and Z_T in equation 13 are close. Therefore, the magnitude of the first (proportional to Z_T) term in equation 10 is typically much greater than that of the second (proportional to $Z_T - Z_N$) term. This observation allowed Kachanov (1980; 1992) to state that the influence of fractures on the effective elasticity is largely controlled by the first term in equation 10 or by the second-rank crack-density tensor,

$$\alpha_{ij} = \frac{1}{V} \sum_k \left(a^3\, n_i\, n_j\right)^{(k)} \quad (i,\, j = 1,\, 2,\, 3)\,, \qquad (14)$$

whose trace, $\mathrm{tr}\, \boldsymbol{\alpha} = e$, coincides with the conventional crack density e for a single fracture set.

As a consequence, a solid with *arbitrarily oriented* circular dry cracks is nearly *orthorhombic* (or orthotropic), and the axes of crack-induced orthotropy approximately coincide with the principal directions of tensor $\boldsymbol{\alpha}$. This conclusion of the non-interaction theory was numerically confirmed by Grechka and Kachanov (2006a; 2006b) both for strongly interacting and intersecting circular fractures. Their computations resulted in the effective stiffness tensors $\boldsymbol{c}_e$ that deviated from orthotropy by less than 1.5% in the entire range of the crack densities expected in naturally fractured reservoirs.

2.2 Dry Irregular cracks

We emphasize that the effective orthotropy is rooted in the closeness of the normal and shear fracture compliances. Such a closeness is not obvious for irregularly-shaped cracks because their shear compliance,

$$Z_T(\phi) \equiv Z_{rr}\, \cos^2 \phi + Z_{tt}\, \sin^2 \phi\,, \qquad (15)$$

depends on the azimuth ϕ within the fracture plane (measured from the direction of eigenvector $\boldsymbol{r}$). This dependence is caused by generally different eigenvalues Z_{rr} and Z_{tt} of tensor $\boldsymbol{Z}$. However, for solids with *multiple* irregular cracks whose in-plane orientations are *random* and *uncorrelated* to their shapes, individual values of Z_{rr} and Z_{tt} no longer matter, and, instead, the average in-plane shear compliance,

$$\langle Z_T \rangle = \frac{1}{2\,\pi} \int_0^{2\,\pi} Z_T(\phi)\, d\phi = \frac{Z_{rr} + Z_{tt}}{2}\,, \qquad (16)$$

becomes important. It is this quantity that should be compared to Z_N to make an inference about proximity of the overall symmetry of rocks with irregular cracks to orthotropy.

In fact, an indication that the effective orthotropy might hold with a good accuracy for solids with multiple differently oriented cracks was recently given by Sevostianov and Kachanov (2002). They examined elliptic fractures and found that their average shear compliance $\langle Z_T \rangle$ deviated from that of equivalent circular cracks by mere 0.7% when the ellipses' eccentricity was 2 and by 3.2% when the eccentricity was 58. The results of Sevostianov and Kachanov (2002) prove that elliptic cracks can be accurately approximated by the circular ones when the ellipses are randomly oriented. As analytic expressions for tensor $\boldsymbol{Z}$ are available only for elliptic fractures (circles are a special case of ellipses), numerical techniques remain the only option for finding out whether effective elasticity of rocks with *arbitrarily-shaped* fractures can be represented by those containing circular cracks.

3 FINITE ELEMENT MODELING

We constructed a number of digital rocks that have cracks of various shapes and examined their influence

on the effective elasticity. Here we discuss our models (Figure 1) that, we believe, exhibit enough variability to make our results conclusive. We performed finite element computations [implemented with Femlab (2003) software] that aim at

- calculating the ratios $Z_T(\phi)/Z_N$ and $\langle Z_T\rangle/Z_N$ for a single fracture;
- obtaining the stiffness contributions $\Delta\boldsymbol{c}$ for a single set of irregular fractures that have random in-plane orientations; and
- computing the effective stiffness and anisotropic coefficients for models with several sets of vertical, intersecting, non-circular cracks.

3.1 Z_T/Z_N ratios for irregular fractures

Let us begin with numerical analysis of the normal and shear compliances for irregular cracks. Examination of the closeness Z_T and Z_N involves the following steps:

(1) Fracture geometries and parameters of their infill and the background need to be specified. Our crack geometries are shown in Figure 1. The fractures are dry. The host rock is isotropic; it has the P-wave velocity $V_{P,\,b} = 3.0$ km/s, the S-wave velocity $V_{S,\,b} = 1.0$ km/s, and the density $\rho_b = 2.2$ g/cm^3. This makes the background Young's modulus $E = 6.33$ GPa and the Poisson's ratio $\nu = 0.44$.

(2) Next, we set up the boundary conditions. They are the remote loads

$$\boldsymbol{T} = T\,[\,0,\,\cos\phi,\,\sin\phi\,]$$

in directions tangent to the fracture plane $[\boldsymbol{x}_2,\,\boldsymbol{x}_3]$. Here ϕ is the in-plane azimuth measured from the $\boldsymbol{x}_2$-axis in Figure 1, and T is a scalar measured in Pa.

(3) Then we solve the elastic equilibrium equations with the finite element method and find the in-plane components of displacement discontinuities $[u_j]$ ($j = 2,\,3$). Averaging them over the fracture area A results in components $b_j = \langle[u_j]\rangle$.

(4) The next and final step in calculating the shear compliance is to combine components b_2 and b_3 into $b(\phi) = b_2\cos\phi + b_3\sin\phi$. According to definition 7, this yields

$$b(\phi) = T\,(Z_{22}\,\cos^2\phi + 2\,Z_{23}\,\cos\phi\,\sin\phi + Z_{33}\,\sin^2\phi)\,,$$

$$b(\phi) \equiv T\,Z_T(\phi)\,.$$

(5) To obtain the normal crack compliance Z_N, we specify the normal boundary load $\boldsymbol{T} = T\,[\,1,\,0,\,0\,]$ and compute (again, with the finite element method) the jump $[u_1]$ and its areal average $b_1 = \langle[u_1]\rangle$. Applying equation 7, we get

$$b_1 = T\,Z_N\,.$$

The procedure we just described gives the crack compliances Z_N and $Z_T(\phi)$ for all fracture geometries displayed in Figure 1. To make their comparison more transparent, we compute the ratios

$$R(\phi) = \Big(1 - \frac{\nu}{2}\Big)\,\frac{Z_T(\phi)}{Z_N}\,. \tag{17}$$

These ratios $R(\phi) \equiv 1$ for circular cracks (equation 13), therefore, any deviation of $R(\phi)$ from unity is a consequence of the fracture non-circularity. If the cracks are oriented randomly within their planes, however, not $R(\phi)$ as such but rather its orientational average, $\langle R\rangle$, is the measure of their cumulative influence on the effective elasticity. We examine both $R(\phi)$ and $\langle R\rangle$ next.

Figure 2 displays ratios $R(\phi)$ (solid symbols) and $\langle R\rangle$ (same symbols but open) for fracture geometries in Figure 1. It leads to the following observations:

- The magnitude of variation $R(\phi)$ naturally depends on the fracture elongation. Perhaps this is why our rectangular crack (model 1 in Figure 1) exhibits the greatest variation. On the other hand, the ratio $\max R(\phi)/\min R(\phi)$ for this crack is only 1.5 whereas the ratio of the rectangle sides is 4. This indicates that contributions of irregular cracks to the effective elasticity are closer to those of circular fractures than their geometries would imply.
- All $\langle R\rangle$ in Figure 2 are greater than one. This suggests that circles have the closest Z_N and $\langle Z_T\rangle$ among all other shapes.
- While all $\langle R\rangle > 1$, their deviations from the unity are not large. The greatest $\langle R\rangle = 1.22$ for model 6 in Figure 1, the second greatest $\langle R\rangle = 1.17$ for the rectangular crack (model 1). We could not establish any meaningful correlations between the values of $\langle R\rangle$ and fracture shapes; partial contacts of the fracture faces (models 4, 5, 6) do not seem to matter.

The fact that $\langle R\rangle > 1$ for all examined irregular fractures indicates that relative magnitude of the second (proportional to $Z_T - Z_N$) term in equation 10 grows when a crack becomes non-circular. Potentially, it can cause some deviations of the effective symmetry from orthotropy when multiple fracture sets are present. (We remind a reader that the effective orthotropy in the non-interaction approximation rests on equality $Z_T = Z_N$.) There are two reasons, however, that prevent these deviations from being significant. First, the compliances Z_T and Z_N are still close to each other for irregular cracks even though their difference $Z_T - Z_N$ is somewhat larger than that for circular fractures. Second, two terms in equation 10 have different signs. Therefore, the overall contribution of cracks to the effective elasticity decreases when the $(Z_T - Z_N)$-term grows. Consequently, the effective media become more isotropic, and their orthotropy turns out to be well justified again. Grechka and Kachanov (2006a) confirmed this statement numerically for liquid-filled cracks, where $Z_T \approx Z_T^{\rm dry}$ and $Z_N \approx 0$. Thus, Figure 2 suggests that we cannot expect irregular dry cracks to cause strong deviations of the effective symmetry from orthotropy.

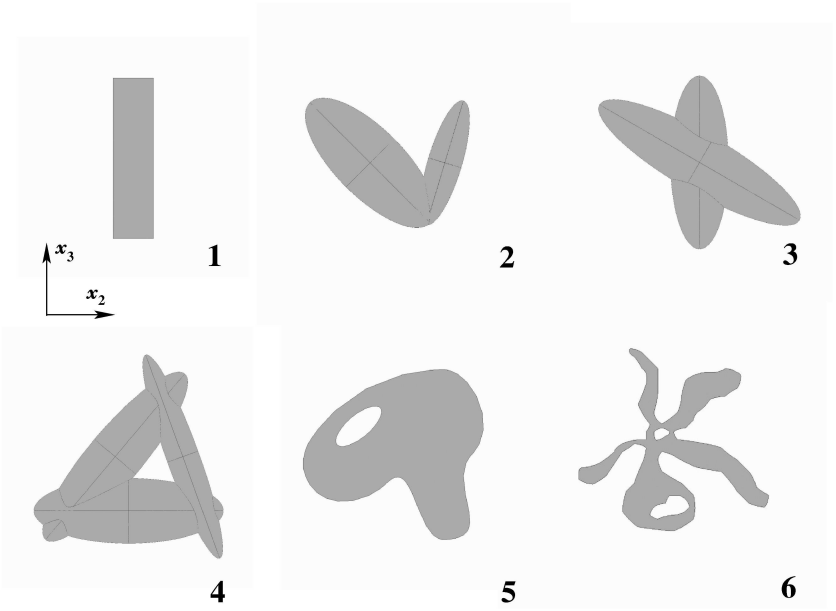

Figure 1. Fracture geometries used to study the influence of crack shape on the effective properties. All fractures are vertical and planar; their normals are directed along the $\boldsymbol{x}_1$-axis. Geometries 4, 5, and 6 contain rock islands inside the cracks; these models represent partially closed fractures.

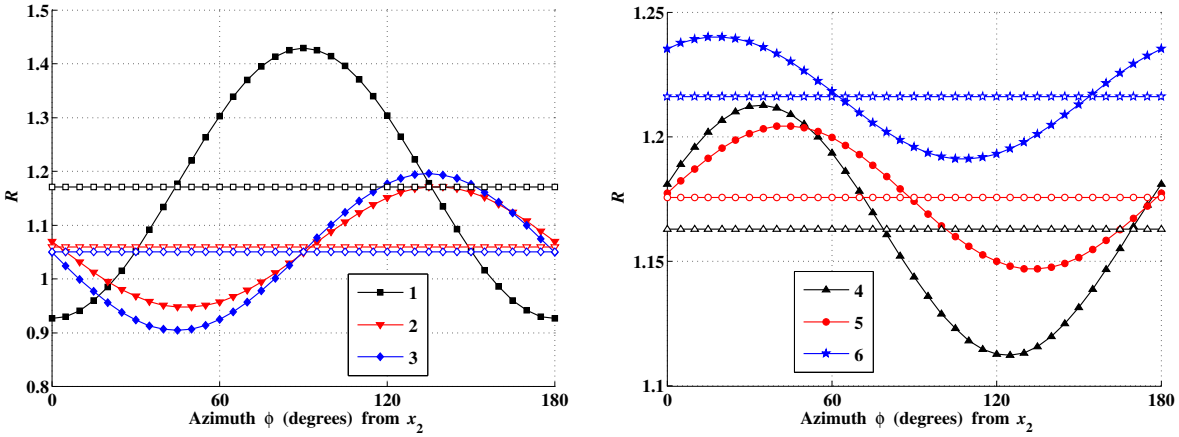

Figure 2. $R(\phi)$ (solid symbols) and $\langle R \rangle$ (open symbols) for fracture models 1 through 6 shown in Figure 1.

3.2 Closeness of irregular and circular cracks

The conclusion drawn in the previous section is entirely based on the closeness of the compliance ratios $\langle Z_T \rangle / Z_N$ for circular and irregularly-shaped cracks. Here we substantiate it by finding the actual crack densities of penny-shaped fractures that fit the cumulative contribution of the irregular, randomly oriented cracks to the effective elasticity.

We organize our computations as follows:

(1) For each fracture shape displayed in Figure 1, we compute the effective stiffness tensor $\boldsymbol{c}_e^{\,\mathrm{N}}$ (see Grechka, 2003; 2005; here we use both the traction and displacement boundary conditions to verify the accuracy of our computations). The superscript "N" in $\boldsymbol{c}_e^{\,\mathrm{N}}$ stands to indicate that these stiffness tensors come from numerical (finite element) simulations.

(2) Next, we average $\boldsymbol{c}_e^{\,\mathrm{N}}$ over the fracture in-plane azimuths according to equation

$$\langle c^{\mathrm{N}}_{e,\,ijkl} \rangle = \frac{1}{2\,\pi} \int_0^{2\,\pi} \Phi_{ii'}(\phi)\, \Phi_{jj'}(\phi)\, \Phi_{kk'}(\phi)\, \Phi_{ll'}(\phi)\, c^{\mathrm{N}}_{e,\,i'j'k'l'}\, d\phi \tag{18}$$

$$(i,\, j,\, k,\, l = 1,\, 2,\, 3)\,,$$

where the rotation matrix $\mathbf{\Phi}(\phi)$ is

$$\mathbf{\Phi}(\phi) = \begin{pmatrix} 1 & 0 & 0 \\ 0 & \cos\phi & \sin\phi \\ 0 & -\sin\phi & \cos\phi \end{pmatrix}.$$

Having computed $\langle \boldsymbol{c}_e^{\,\mathrm{N}} \rangle$, it is straightforward to get the crack contributions to the effective stiffness,

$$\langle \Delta \boldsymbol{c}^{\,\mathrm{N}} \rangle = \langle \boldsymbol{c}_e^{\,\mathrm{N}} \rangle - \boldsymbol{c}_b \,. \tag{19}$$

(3) Finally, we fit our $\langle \Delta \boldsymbol{c}^{\,\mathrm{N}} \rangle$ with theoretical stiffness contributions $\Delta \boldsymbol{c}^{\,\mathrm{ps}}(e^{\,\mathrm{fit}}, \theta)$ that correspond to a single set of circular, penny-shaped cracks and come from a non-interaction scheme that accounts for a finite fracture aspect ratio θ (Kachanov et al., 2003, p. 259). Both the crack density $e^{\,\mathrm{fit}}$ and θ are the fitting parameters; they are obtained from the nonlinear optimization $\langle \Delta \boldsymbol{c}^{\,\mathrm{N}} \rangle \sim \Delta \boldsymbol{c}^{\,\mathrm{ps}}(e^{\,\mathrm{fit}}, \theta)$.

The described sequence of computations makes it possible to examine the stiffness misfits,

$$\Delta_{\,c} = \langle \Delta \boldsymbol{c}^{\,\mathrm{N}} \rangle - \Delta \boldsymbol{c}^{\,\mathrm{ps}} \,, \tag{20}$$

resulting from the approximation of irregular fractures with penny-shaped ones. Note that we are intentionally comparing the stiffness *contributions*, $\Delta \boldsymbol{c}$, rather than the effective stiffness tensors, $\boldsymbol{c}_e$, themselves. The latter obviously depend on the crack density or the degree of fracturing while the former are free from such a dependence.

To get quantitative estimates of the magnitudes of misfits Δ_c, we calculate their ℓ_1 norms

$$\Delta_{\,c}^{\,\mathrm{nrm}} = \frac{\max|\Delta_{\,c}|}{\max|\langle \Delta \boldsymbol{c}^{\,\mathrm{N}} \rangle|} \times 100\% \,. \tag{21}$$

Figure 3 demonstrates that the misfits $\Delta_{\,c}^{\,\mathrm{nrm}} < 0.7\%$ for all our fracture geometries. The reason of why these misfits are much smaller than deviations of $\langle R \rangle$ from unity (Figure 2) is explained in Appendix A. Clearly, our irregular fractures can be accurately represented by penny-shaped ones. Thus, our conclusion coincides with that of Sevostianov and Kachanov (2002) for elliptic cracks and extends their result further to *arbitrarily-shaped* fractures.

Our computations result in an important quantity – the crack density $e^{\,\mathrm{fit}}$ of the best-fit penny-shaped fractures. We now compare $e^{\,\mathrm{fit}}$ with the crack-density parameter

$$e^{\,\mathrm{ell}} = \frac{2}{\pi V} \sum_k \left(\frac{A^2}{P} \right)^{(k)} \tag{22}$$

introduced by Budiansky and O'Connell (1976). In the equation above, A and P are the crack area and perimeter, respectively, and the summation is performed over all fractures k in the representative rock volume V. Figure 4 shows the ratios $e^{\,\mathrm{fit}}/e^{\,\mathrm{ell}}$ for our crack geometries. Overall, the accuracy of equation 22 is not high: $e^{\,\mathrm{ell}}$ deviates from $e^{\,\mathrm{fit}}$ by as much as 25%. These deviations are expected to grow for cracks with small areas of partial contacts that leave both A and P, and, therefore, $e^{\,\mathrm{ell}}$ virtually unchanged but can significantly reduce the crack compliance (Sevostianov and Kachanov, 2002).

3.3 Multiple sets of non-circular cracks

Finally, we directly examine the effective elasticity due to multiple, non-circular, intersecting fractures. For this test, we create a suite of models containing three sets of vertical, dry, rectangular cracks that have the shapes identical to crack 1 in Figure 1. The azimuths of the sets are $\varphi_1 = 0^\circ$, $\varphi_2 = 40^\circ$, and $\varphi_3 = 60^\circ$ with respect to the coordinate axis $\boldsymbol{x}_1$. Each set has 5 cracks rotated around their normals with 36° increment to remove any preferential in-plane fracture orientation; each model contains 15 fractures. The locations of their centers are random in the representative volume V and uncorrelated to the in-plane crack rotations. The crack densities of our fracture sets [computed in accordance with equation 22 which is reasonably accurate for rectangular shapes (Figure 4)] are $e_1 = 0.04$, $e_2 = 0.03$, and $e_3 = 0.02$; they make the cumulative crack density $e = 0.09$.

It is virtually impossible to place the above described fractures in V randomly and avoid their intersections, so all our models contain intersecting cracks. Sometimes relatively few fractures intersect (Figure 5a), sometimes many (Figure 5b), sometimes all, forming a single interconnected fracture network (Figure 5c). Fracture arrays shown in Figure 5 exhibit a high level of three-dimensional geometrical complexity. Specifically, the fracture shapes are non-circular, their faces are not smooth because the cracks often protrude through each other, and there are irregular pieces of host rock between the cracks owing to complicated geometry of their intersections.

As all fractures are vertical and all in-fracture-plane directions are equivalent, the effective symmetry is monoclinic with a horizontal symmetry plane. Figure 6 displays the effective anisotropic coefficients (introduced for monoclinic media by Grechka et al., 2000) computed with either traction or displacement boundary conditions for 20 random realizations of the fracture locations. The most important feature of Figure 6 is that vastly diverse geometries of intersecting fractures do *not* cause significant variability in the effective anisotropic coefficients. This means that (1) crack intersections do not contribute to the effective elasticity, and (2) only 15 fractures are sufficient for volume V to be *representative* for the elastic properties. Both these conclusions have been drawn for circular cracks by Grechka and Kachanov (2006b). The absence of the influence of crack intersections on the effective properties was also pointed out by Saenger et al. (2004), who performed the wave-propagation rather than static numerical experiments for models containing up to 2000 fractures.

Figure 6 has two more features of interest:

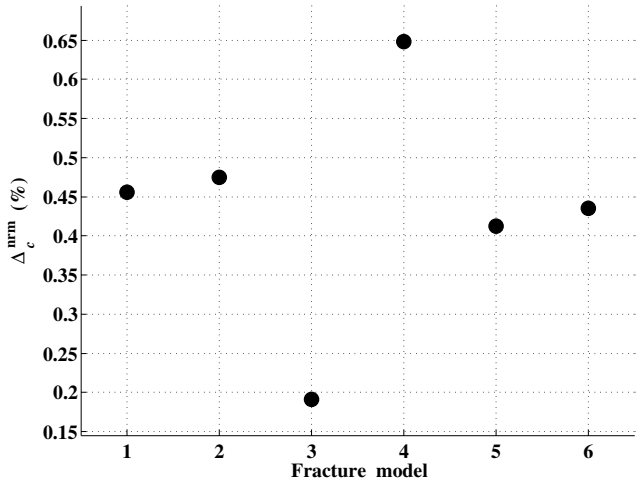

Figure 3. Misfits Δ_c^{nrm} (equation 21) for six fracture shapes in Figure 1.

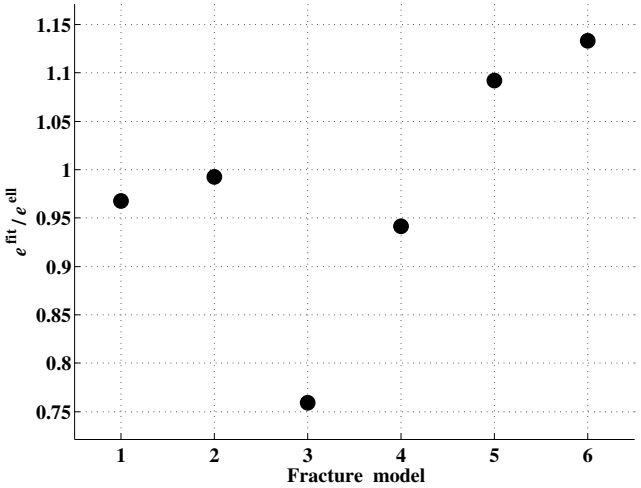

Figure 4. Ratios $e^{\mathrm{fit}}/e^{\mathrm{ell}}$ for fractures in Figure 1.

• All anellipticity coefficients η are small: $\max|\eta^{(1)}| = 0.015$. Therefore, the effective anisotropy is elliptical for practical purposes because such η values can be hardly detected from seismic data. This is also the case for multiple sets of dry circular cracks.

• The maximum of ζ-coefficients, which quantify the deviation of monoclinic symmetry from orthotropy, is 0.005. Clearly, the effective anisotropy is orthorhombic given typical errors in estimating anisotropy from seismic data.

The last point can be substantiated by calculating the relative ℓ_1 norms of the deviations of numerically computed effective stiffness tensors $\boldsymbol{c}_e^{\mathrm{N}}$ from orthotropy. Similarly to Grechka and Kachanov (2006a), we define

$$\Delta^{\mathrm{ort}} = \frac{\max|\boldsymbol{c}_e^{\mathrm{N}} - \boldsymbol{c}_e^{\mathrm{ort}}|}{\max|\boldsymbol{c}_e^{\mathrm{N}}|} \times 100\%\,, \tag{23}$$

where tensors $\boldsymbol{c}_e^{\mathrm{ort}}$ are obtained from $\boldsymbol{c}_e^{\mathrm{N}}$ by letting

$$c_{e,\,ijlm}^{\mathrm{ort}} = \begin{cases} 0 & \text{when} \quad \delta_{ij}\,\delta_{lm} + \delta_{il}\,\delta_{jm} + \delta_{im}\,\delta_{jl} = 0 \quad \text{and} \\ c_{e,\,ijlm}^{\mathrm{N}} & \text{otherwise,} \quad (i,\,j,\,l,\,m = 1,\,2,\,3)\,. \end{cases} \tag{24}$$

Figure 7 shows that all relative norms Δ^{ort} are less than 1%, therefore, the effective anisotropy is virtually orthorhombic as if the cracks were non-intersecting and non-interacting.

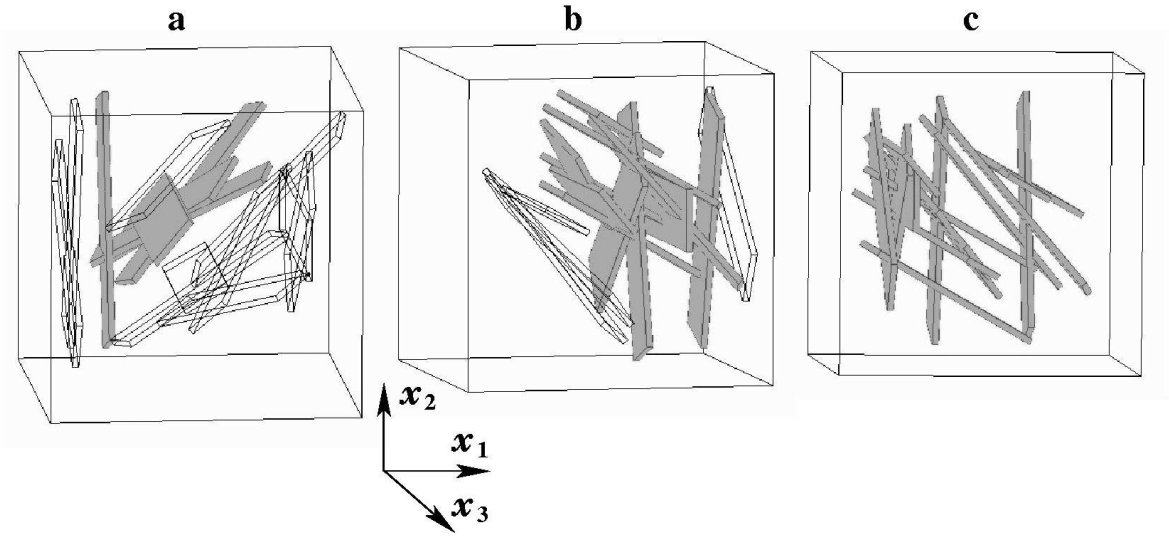

Figure 5. Models containing three sets of vertical rectangular cracks. Fractures that geometrically intersect their neighbors are shaded; isolated cracks are transparent. Cubes represent the rock volumes V indicating that the sizes of fractures and V are comparable.

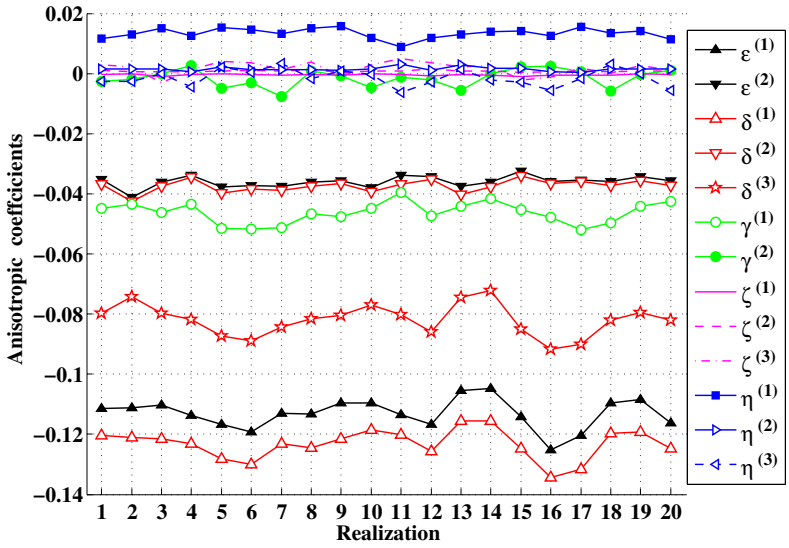

Figure 6. Effective anisotropic coefficients for models that contain three vertical sets of rectangular cracks.

4 DISCUSSION AND CONCLUSIONS

Overwhelming majority of the existing theoretical results for effective elasticity of fractured solids is based on the assumption of unrealistically simple – circular or elliptic – shapes of cracks. Such an assumption naturally raises a question of whether the conventional theories are applicable to rocks characterized by highly irregular, intersecting fractures that are often partially closed. Having recognized this issue, we presented a series of numerical experiments on 3D models (the so-called digital rocks) with unconventional fracture shapes. Our main conclusion is that *contribution to the effective elasticity of multiple sets of irregular, randomly rotated around their normals, planar cracks is indistinguishable from that of their circular counterparts.* Consequently, all well-known theoretical results derived for penny-shaped fractures can be transferred with a good accuracy to flat non-circular cracks.

Specifically, our paper concentrated on three related problems:

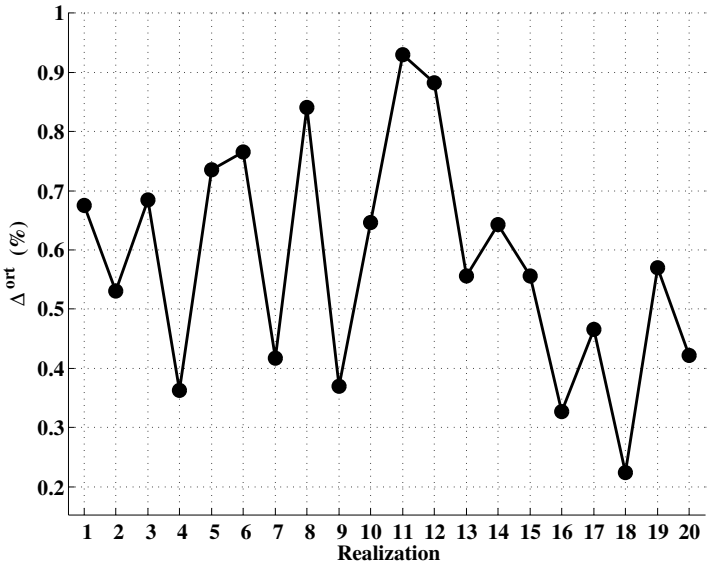

Figure 7. Relative deviations Δ^{ort} of the effective stiffness tensors from orthotropy (equations 23, 24).

• the ratios of the crack compliances $\langle Z_T \rangle / Z_N$ for irregular and circular fractures;

• the accuracy of replacement of non-circular cracks with penny-shaped ones; and

• the effective anisotropy caused by multiple sets of intersecting, irregular, dry fractures.

All three studies demonstrated that even strong deviations of fracture shapes from circles are still insignificant for the overall crack-induced elasticity. In particular, we showed that:

• Even though the ratios $\langle Z_T \rangle / Z_N$ are somewhat higher for dry irregular fractures than Z_T/Z_N for circular ones, they are not nearly high enough to cause noticeable deviations from the effective orthotropy. (As a reminder, the effective orthotropy stems from equality $Z_T = Z_N$, which is an approximation for both circular and arbitrarily-shaped fractures.)

• The stiffness contribution $\Delta \boldsymbol{c}$ of non-circular cracks that have random in-plane orientations can be accurately represented by properly selected penny-shaped fractures. The error caused by this change in the fracture shape is less than 0.7% for all examined fracture geometries.

• Effective elliptical orthotropy, established for multiple sets of dry penny-shaped cracks, holds with the same accuracy for dry fractures that have any shape. In our tests, we let the cracks intersect, protrude through each other, and create interconnected networks. And yet, all deviations from orthotropy turned out to be less than 1%. Also the anellipticity of effective anisotropy (quantified by the η-coefficients) was less that 0.015, which is essentially zero for seismics.

While our numerical simulations clearly indicate that the shape of planar cracks is not a parameter of concern for linearly elastic, inclusion-type fracture models, they give no justification of whether those models are the only ones capable of describing cracks in real rocks. For instance, one of alternative models that represents a dry fracture as a contact of two rough surfaces (e.g., Yoshioka and Scholz, 1989; Baltazar et al., 2002; Biwa et al., 2005) results in somewhat higher $\langle Z_T \rangle / Z_N$ ratios than ours. Therefore, we suggest that more measurements on real fractured rocks, both on laboratory and field scales, are needed to understand the strengths and limitations of various existing approaches.

5 ACKNOWLEDGEMENTS

We thank Shell International E & P Inc. for permission to publish the paper and Jorge Lopez (Shell), Mark Chapman (EAP), and an anonymous reviewer for their suggestions that improved our manuscript. The work presented here was conducted during I.V.'s internship at Shell International E & P, Summer 2005. We also appreciate the many interesting discussions on fracture microcorrugations with Ilya Tsvankin and Rodrigo Fuck, both CWP.

REFERENCES

Baltazar, A., S. I. Rokhlin, and C. Pecorari, 2002, On the relationship between ultrasonic and micromechanical properties of contacting rough surfaces: Journal of the Mechanics and Physics of Solids, **50**, 1397–1416.

Biwa, S., A. Suzuki, and N. Ohno, 2005, Evaluation of interface wave velocity, reflection coefficients and interfacial

stiffnesses of contacting surfaces, Ultrasonics, **43**, 495–502.

Bristow, J. R., 1960, Microcracks and the static and dynamic elastic constants of annealed and heavily cold-worked metals: British Journal of Applied Physics, **11**, 81–85.

Budiansky, B., and R. J. O'Connell, 1976, Elastic moduli of a cracked solid: International Journal of Solids and Structures, **12**, 81–97.

Eshelby, J. D., 1957, The determination of the elastic field of an ellipsoidal inclusion and related problems: Proceedings of Royal Society, **A241**, 376–396.

Femlab Reference Manual, 2003, Comsol, `www.femlab.com`.

Grechka, V., 2003, Effective media: A forward modeling view: Geophysics, **68**, 2055–2062.

Grechka, V., 2005, Penny-shaped fractures revisited: Studia Geophysica et Geodaetica, **49**, 367–383.

Grechka, V., P. Contreras, and I. Tsvankin, 2000, Inversion of normal moveout for monoclinic media: Geophysical Prospecting, **48**, 577–602.

Grechka, V., and M. Kachanov, 2006a, Seismic characterization of multiple fracture sets: Does orthotropy suffice? Geophysics, **71**, in print.

Grechka, V., and M. Kachanov, 2006b, On effective elasticity of rocks with interacting and intersecting cracks: Geophysics, **71**, in print.

Hudson, J. A., 1980, Overall properties of a cracked solid: Mathematical Proceedings of Cambridge Philosophical Society, **88**, 371–384.

Hudson, J. A., 1994, Overall properties of a material with inclusions or cavities: Geophysical Journal International, **117**, 555–561.

Kachanov, M., 1980, Continuum model of medium with cracks: Journal of the Engineering Mechanics Division, ASCE, **106** (EM5), 1039–1051.

Kachanov, M., 1992, Effective elastic properties of cracked solids: Critical review of some basic concepts: Applied Mechanics Review, **45**, 304–335.

Kachanov, M., 1993, Elastic solids with many cracks and related problems. In: Hutchinson, J. W., and T. Wu (Eds.), Advances in Applied Mechanics, **30**, 259–445.

Kachanov, M., B. Shafiro, and I. Tsukrov, 2003, Handbook of Elasticity Solutions, Kluwer Academic Publishers.

Saenger, E. H., O. S. Krüger, and S. A. Shapiro, 2004, Effective elastic properties of randomly fractured soils: 3D numerical experiments: Geophysical Prospecting, **52**, 183–195.

Sayers, C., and M. Kachanov, 1995, Microcrack-induced elastic wave anisotropy of brittle rocks, Journal of Geophysical Research, **100**, B3, 4149–4156.

Schoenberg, M., 1980, Elastic wave behavior across linear slip interfaces: Journal of Acoustical Society of America, **68**, 1516–1521.

Schoenberg, M., and C. Sayers, 1995, Seismic anisotropy of fractured rock: Geophysics, **60**, 204–211.

Sevostianov, I., and M. Kachanov, 2002, On elastic compliances of irregularly shaped cracks: International Journal of Fracture, **114**, 245–257.

Vavakin, A. S., and R. L. Salganik, 1975, Effective characteristics of nonhomogeneous media with isolated inhomogeneities: Mechanics of Solids, Allerton Press, 58–66 (English translation of Izvestia AN SSSR, Mekhanika Tverdogo Tela **10**, 65–75).

Walsh, J. B., 1965a, The effect of cracks on the compressibility of rocks: Journal of Geophysical Research, **70**(2), 381–389.

Walsh, J. B., 1965b, The effect of cracks on uniaxial compression of rocks: Journal of Geophysical Research, **70**(2), 399–411.

Yoshioka, N., and C. H. Scholz, 1989, Elastic properties of contacting surfaces under normal and shear loads. 1. Theory: Journal of Geophysical Research, **94**, B12, 17,681–17,690.

APPENDIX A: SENSITIVITIES OF EFFECTIVE COMPLIANCES AND STIFFNESSES TO Z_N AND Z_T

Here we demonstrate that the fracture compliance contribution, $\Delta\boldsymbol{s}$, is significantly more sensitive to the shear crack compliance Z_T than the stiffness contribution, $\Delta\boldsymbol{c}$. Let us examine a single set of planar, rotationally-invariant fractures that have normals $\boldsymbol{n} = [1, 0, 0]$. The crack contribution to the overall compliance (in Voigt notation) is

$$\Delta\boldsymbol{s} = \begin{pmatrix} Z_N & 0 & 0 & 0 & 0 & 0 \\ 0 & 0 & 0 & 0 & 0 & 0 \\ 0 & 0 & 0 & 0 & 0 & 0 \\ 0 & 0 & 0 & 0 & 0 & 0 \\ 0 & 0 & 0 & 0 & Z_T & 0 \\ 0 & 0 & 0 & 0 & 0 & Z_T \end{pmatrix}. \tag{A1}$$

The corresponding stiffness contribution, $\Delta\boldsymbol{c}$, is most easily evaluated in the linear approximation which is valid when $||\Delta\boldsymbol{s}|| \ll ||\boldsymbol{s}_b||$. Equation 11 then yields

$$\begin{aligned} \Delta c_{ijkl} &= (s_{b,\,ijkl} + \Delta s_{ijkl})^{-1} - c_{b,\,ijkl} \\ &\approx -c_{b,\,iji'j'}\,\Delta s_{i'j'k'l'}\,c_{b,\,k'l'kl} \end{aligned} \tag{A2}$$

$$(i,\,j,\,k,\,l = 1,\,2,\,3)\,,$$

or, in Voigt notation,

$$\Delta\boldsymbol{c} \approx -\mu^2 \begin{pmatrix} \left(\frac{\lambda}{\mu}+2\right)^2 Z_N & \frac{\lambda}{\mu}\left(\frac{\lambda}{\mu}+2\right) Z_N & \frac{\lambda}{\mu}\left(\frac{\lambda}{\mu}+2\right) Z_N & 0 & 0 & 0 \\ \frac{\lambda}{\mu}\left(\frac{\lambda}{\mu}+2\right) Z_N & \left(\frac{\lambda}{\mu}\right)^2 Z_N & \left(\frac{\lambda}{\mu}\right)^2 Z_N & 0 & 0 & 0 \\ \frac{\lambda}{\mu}\left(\frac{\lambda}{\mu}+2\right) Z_N & \left(\frac{\lambda}{\mu}\right)^2 Z_N & \left(\frac{\lambda}{\mu}\right)^2 Z_N & 0 & 0 & 0 \\ 0 & 0 & 0 & 0 & 0 & 0 \\ 0 & 0 & 0 & 0 & Z_T & 0 \\ 0 & 0 & 0 & 0 & 0 & Z_T \end{pmatrix}, \tag{A3}$$

where λ and μ are the background Lamé coefficients.

Comparing equations A1 and A3, we immediately notice the difference. All stiffness elements containing Z_N in equation A3 have the multipliers that depend on the λ/μ ratio. The magnitudes of these factors can be evaluated bearing in mind that typical velocity ratios $V_{P,\,b}/V_{S,\,b} = \sqrt{\lambda/\mu + 2}$ in rocks have the values $2 \lesssim V_{P,\,b}/V_{S,\,b} \lesssim 3$ (they correspond to the Poisson's ratios $0.33 \lesssim \nu \lesssim 0.45$). This makes the factors in equation A3 lie between 4 and 81.

For dry cracks, the compliances Z_N and Z_T are comparable, therefore, they equally contribute to the norm of $\Delta\boldsymbol{s}$ given by equation A1. In contrast, the norm $||\Delta\boldsymbol{c}||$ is primarily governed by Z_N because of the large prefactors in equation A3 and, consequently, it is relatively insensitive to both Z_T and $Z_T - Z_N$ for a given Z_N. As the difference $Z_T - Z_N$ determines the accuracy of replacement of irregular fractures with penny-shaped ones, such a replacement is much more accurate if evaluated in terms of $\Delta\boldsymbol{c}$ than in terms of $\Delta\boldsymbol{s}$. This result has an important implication for seismics. Being functions of the effective stiffnesses rather than compliances, the seismic velocities and other signatures inherit a low sensitivity of the former to the fracture shapes.